"Cherry-Pit" Structures in Binary Immiscible Alloy Under Ion Irradiation

Shipeng Shu, Kenneth Tussey

May 8, 2011

Abstract

We study an special microstructure (matrix atom riched small clusters inside the solute riched precipitate, the so-called "cherry-pit" structure) observed in some binary alloys under ion irradiation. Asymmetry phase diagram is constructed by introducing triplet atomic interaction. KMC simulation is used to see whether the "cherry-pit" structure can be observed on both sides of the phase diagram. Cluster mobility is also measured by KMC simulation in order to explain the formation of such structure. Our result suggest that a low enough "pit" atom mobility is crucial for the formation of the structure. The ballistic jump frequency is also an important parameter for such microstructure to be observed.

1 Introduction

Ion irradiation on materials will lead to various effects, including point defects production, forced atomic mixing of alloy components, etc. When supersaturated immiscible alloy system is quenched into the miscibility gap, precipitate will form and grow in size. Under ion irradiation, however, the system cannot evolute all the way to the thermal equilibrium state, because of the forced mixing of alloy components. The competition between thermodynamics, which will drive the system to phase separation, and ion irradiation, which will drive the alloy into random solution, will lead to different microstructures within the system.

Recently, Stumphy and colleagues have observed small matrix atoms riched precipitates appearing in the normal solute riched precipitates in both Cu-Fe systems and Cu-V systems under ion irradation, using a three-dimensional atom probe[1]. This unusual microstructure (we call it Cherry-Pit structure) is obviously a result of ion irradiation.

Both Cu-Fe and Cu-V alloy system have significantly asymmetric phase diagram. In addition, the cohesive energy of the solvent and solute atoms are also different, so that Cu atom mobility in Fe matrix is different from Fe mobility in Cu matrix, and the same thing happens for the Cu-V alloy.

In this paper, we would like to use kinetic Monte Carlo simulation to rationalize the formation and evolution of the "Cherry-Pit" structure, mainly considering the phase diagram and atom mobility asymmetry of the system.

The paper is organized as follows. In Sec. 2 we briefly show the experimental result. In Sec. 3 we present the atomic diffusion model and kinetic Monte Carlo algorithm. We show the effect of the phase diagram asymmetry on the formation of "Cherry-Pit" structure in

Sec. 4.1, and the effect of asymmetry of cohesive energy in Sec. 4.2. In Sec. 5, a summary is given.

2 Experimental Observation

Stumphy *et al.*[1] used atomic probe tomography (APT) to investigate the 3-D microstructure of dilute $Cu_{1-x}Fe_x$ and $Cu_{1-x}V_x$ ($x \approx 12$) alloy under 1.8 MeV Kr^+ irradiation.

A number of clusters with reduced Fe composition are located inside of the large Fe precipitates shown in the voxel reconstructions in Fig.1. As stated previously, we call such structure "Cherry-Pit" structure, with the Fe precipitate being the "cherry", and the Cu richer clusters inside the Fe precipitate as the "pit".

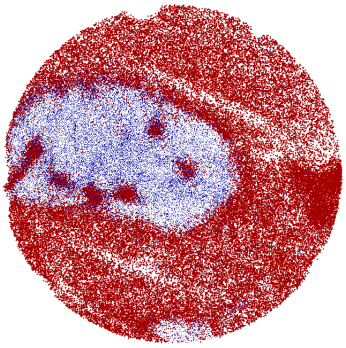

Figure 1: A 1-nm thick layer of atoms from the $3.0 \times 10^{16} ions/cm^2$ dose sample at 350°C. The Fe atoms (blue) have been minimized to make the Cu atoms (red) located inside of the large Fe precipitate more visible. The diameter of the layer is 52nm.

For Cu-V sample, the "Cherry-Pit" structures are more obvious, as shown in Fig.2.

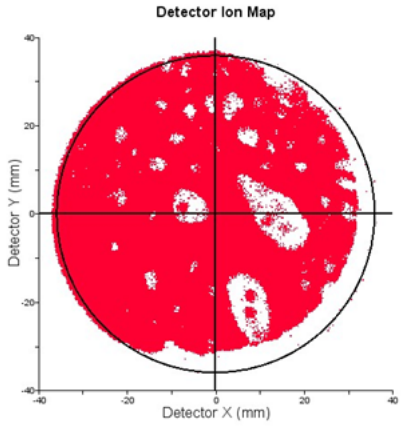

Figure 2: A Cu-V tip that was pre-irradiated at RT to a dose of $5 \times 10^{15} ions/cm^2$, then irradiated at 450°C an additional dose of $3 \times 10^{16} ions/cm^2$.

3 Atomistic KMC model

3.1 Interacting energies

We consider an A-B binary alloy with a highly diluted vacancy V concentration on a rigid lattice with a face-centered-cubic structure. There are $N = L^3$ atomic sites in the simulation box, where we use L to be 32 or 64 in the simulation. Periodic boundary condition is applied to get reasonable bulk properties. There is only one vacancy in the simulation box, and we use the real equilibrium bulk vacancy concentration to rescale the time in order to obtain correct kinetics.

Several energies are included in the simulation. Cohesive energies, $\epsilon_{AA}, \epsilon_{BB}$ and ϵ_{AB}, are the interatomic potential between A-A, B-B, and A-B pairs. the vacancy formation energy, $\epsilon_{AV}, \epsilon_{BV}$, are defined as how much cohesive energy is needed to form a vacancy. If this value is positive, that means energy is needed when forming a vacancy. The pairwise ordering energy, defined as $\epsilon = \epsilon_{AA} + \epsilon_{BB} - 2\epsilon_{AB}$, is the energy difference between fully ordered and disordered states. With pairwise interaction only, if we set $\epsilon_{AA} = \epsilon_{BB}$, the mobility of an A atom in B matrix is equal to that of B atom in A matrix. If we make these two cohesive energies different, we will get so called mobility asymmetry.

Here in this work, in order to construct asymmetric phase diagram, triplet atomic interactions are also considered. If there is three atoms forming a triangle, we also assign an energy to that triangle. these energies are $\epsilon_{AAA}, \epsilon_{AAB}, \epsilon_{ABB}$ and ϵ_{BBB}. By applying the triplet interaction energies, we will get different mixing enthalpy with different alloy compositions. Therefore we can make the phase diagram asymmetrical.

Other important parameters are related to the ion irradiation effects. The forced mixing and disordering as a result of ion irradiation is introduced by forcing exchanges of atoms in the cascade[2]. The first parameter is the ballistic jump frequency, Γ_b, which is a measurement of disordering rate. The other parameters include the relocation distance, and the relocation mode. The distribution of atom relocation can be modeled as gaussian, exponential decay, or just random atomic relocation happening between nearest-neighbors[3]. Here in this work, we apply the exponential decay model, following the results of Enrique *et al.*[4]

3.2 Vacancy jump model

The activation energy for an X-V exchange is derived from a broken bond model[5], for which $\mathscr{E}^{act}_{XV} = \mathscr{E}^{saddle} - \mathscr{E}^{init}$. $\mathscr{E}^{saddle}$ and $\mathscr{E}^{init}$ are the energies at saddle point and in the initial configuration, respectively. The frequency of the X-V exchanges $\nu \propto \nu_0 \exp\{-\beta \mathscr{E}^{act}_{XV}\}$.

4 Simulation results

4.1 Construction of asymmetric phase diagram

We would like to find out whether the asymmetry of the phase diagram will affect the formation of the "cherry-pit" structures. We want to answer the question: will such structures be observed on both sides of the phase diagram?

First we construct the asymmetric phase diagram using both pairwise and triplet interaction. To do this, we try to apply semi-grand canonical Monte Carlo (SGMC) method. To conduct a simi-grand canonical simulation for binary alloy, we sample from all configurations

and compositions for a constant number of atoms[6]. During the simulation, we randomly choose an atom to change the identity of the atom, then we calculate the new energy and chemical potential, and accept the change with a probability of p_{acc}[7]:

$$p_{acc} = min\{1, \exp(-\beta[U_{new} - U_{old} - (\mu_{new} - \mu_{old})])\}$$

In the simulation, we set pairwise ordering energy $\epsilon = 0.0553eV$, triplet interaction $\epsilon_{AAA} = 0.005eV, \epsilon_{BBB} = -0.005eV, \epsilon_{AAB} = \epsilon_{ABB} = 0$. We set $\epsilon_{AAA} = -\epsilon_{BBB}$ so that the triplet interactions just serve as a asymmetry parameter.

A typical result of a semi-grand canonical simulation at T=0.04eV is plotted as Fig.3. We observe a hysteresis phenomena. Both curves have a meta-stable part. In addition, for the asymmetric case, the phase transition does not happen when $\mu = 0$. Therefore, we cannot just take composition of $\Delta\mu = 0$ as a point of the coexistence line of the phase diagram. With Fig.3, we can only obtain the range of the real transition point.

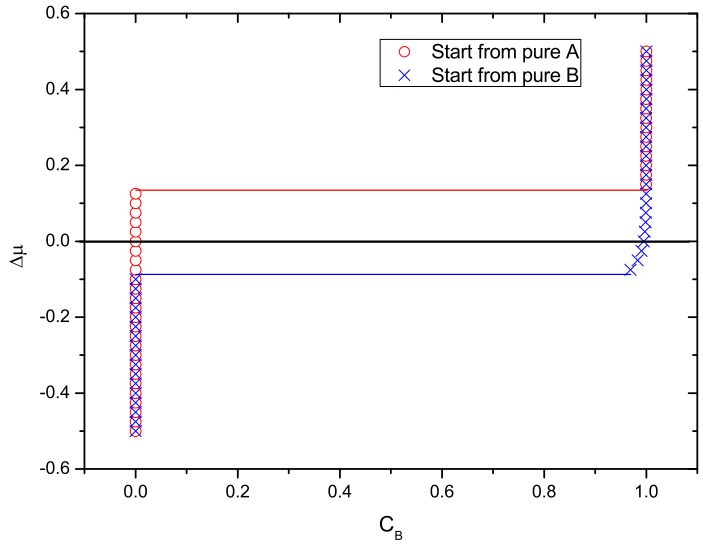

Figure 3: The hysteresis of phase diagram calculation. T=0.04eV. Two simulations are run. One starts from all the atoms to be A type(red), the other from all B atoms(blue).

If we have the full curve of the $\Delta\mu - Composition$ plot, we can determine the exact transition line by using the Maxwell tie-line. Therefore, we try to use the mean field theory

to make an approximation. First we calculate the μ value:

$$\begin{aligned}\mu = & -\frac{1}{2}Z_p C_B\epsilon + \frac{1}{2}Z_p(1-C_B)\epsilon \\ & -\frac{1}{6}Z_t C_B(-3\epsilon_{AAA} - 3\epsilon_{BBB} + 3\epsilon_{AAB} \\ & + 3\epsilon_{ABB} + (1-2C_B)(-\epsilon_{AAA} + \epsilon_{BBB} + 3\epsilon_{AAB} - 3\epsilon_{ABB})) \\ & + \frac{1}{6}Z_t(1-C_B)(-3\epsilon_{AAA} - 3\epsilon_{BBB} + 3\epsilon_{AAB} + 3\epsilon_{ABB} \\ & + (1-2C_B)(-\epsilon_{AAA} + \epsilon_{BBB} + 3\epsilon_{AAB} - 3\epsilon_{ABB})) \\ & + \frac{1}{6}Z_t(1-C_B)C_B(2\epsilon_{AAA} - 2\epsilon_{BBB} - 6\epsilon_{AAB} + 6\epsilon_{ABB}) \\ & - T(k\ln(1-C_B) - k\ln(C_B))\end{aligned}$$

And then calculate $\frac{d\mu}{dC_B}$:

$$\begin{aligned}\frac{d\mu}{dC_B} = & -Z_p\epsilon - \frac{1}{3}Z_t(-3\epsilon_{AAA} - 3\epsilon_{BBB} + 3\epsilon_{AAB} \\ & + 3\epsilon_{ABB} + (1-2C_B)(-\epsilon_{AAA} + \epsilon_{BBB} + 3\epsilon_{AAB} - 3\epsilon_{ABB})) \\ & - \frac{1}{3}Z_t C_B(2\epsilon_{AAA} - 2\epsilon_{BBB} - 6\epsilon_{AAB} + 6\epsilon_{ABB}) \\ & + \frac{1}{3}Z_t(1-C_B)(2\epsilon_{AAA} - 2\epsilon_{BBB} - 6\epsilon_{AAB} + 6\epsilon_{ABB}) \\ & - T(-k/(1-CB) - k/C_B)\end{aligned}$$

Z_p and Z_t are the number of nearest neighbors (nearest neighbor triangles for triplet interaction). C_B is the B component composition.

Then we calculate a tie line using $\frac{d\mu}{dC_B}$. The intersections of the tie line and the $\frac{d\mu}{dC_B}$ curve give the coexistence curve, as shown in Fig.4. In Fig.4 we also plot the semi grand canonical results. On the left size, the hysteresis is not significant. However, on the right side of the phase diagram, we see the low and high limit of the semi grand canonical coexistence curve clearly.

As we can see from Fig.4, especially at low temperatures, the MFA theory give good result.

4.2 "Cherry-pit" structures on different sides of the phase diagram

Here we would like to reproduce the "cherry-pit" structure on one side of the phase diagram, and then see whether the same structure will also be observed on the other side, using the same parameters.

To reproduce the "cherry-pit" structure on the left side of the phase diagram (see Fig.4), we run a KMC simulation for $A_{85}B_{15}$ alloy, and change Γ_b. Simulation temperature is set as T=0.036eV. The energy parameters used in the simulation is tabulated in Table1. Here we always set $\epsilon_{BBB} = -\epsilon_{AAA}$, so we only tabulate ϵ_{AAA}.

We ran simulations with Γ_b varies from $0.01s^{-1}$ to $100s^{-1}$. We first find the Γ_b that will lead to "" "cherry-pit" structures, and then use the same Γ_b to ran simulations for $A_{15}B85$ alloy. Typical configurations are shown in Fig.5.

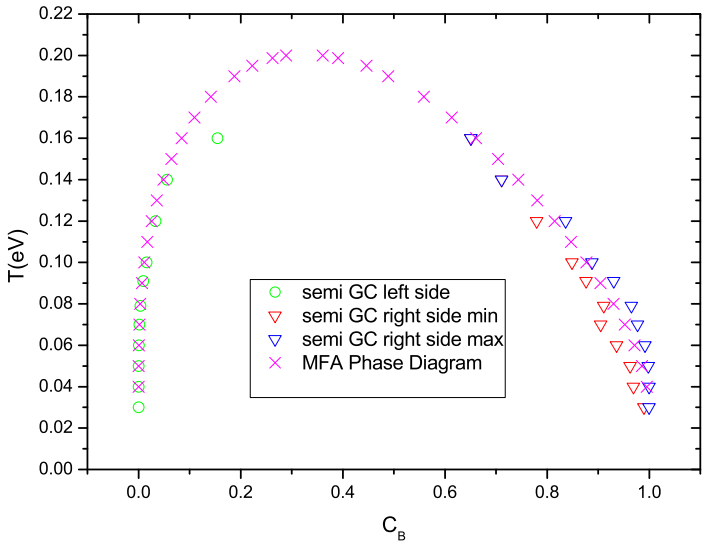

Figure 4: Phase diagram calculated by both MFA and semi grand canonical method.

	ϵ^{order}	ϵ^{coh}	ϵ_V^f	ϵ^{saddle}	ϵ_{AAA}
$A_{85}B_{15}$	0.0553eV	-4.34eV	1.28eV	-10.217eV	0.005eV

Table 1: All the energy parameters for KMC model.

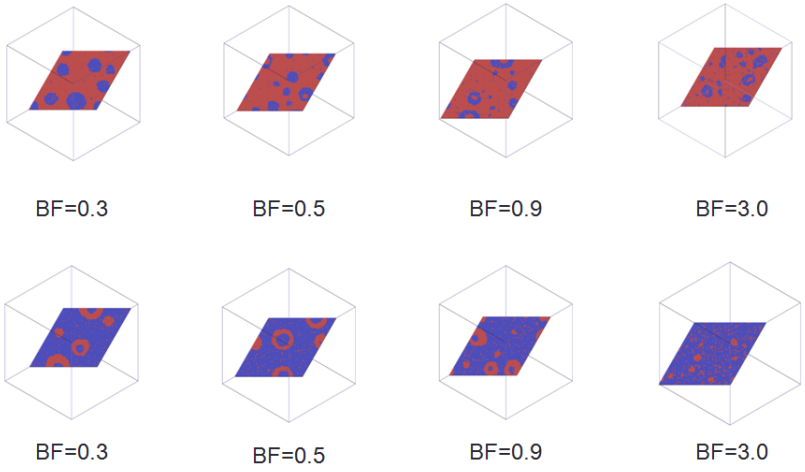

Figure 5: Typical microstructure configurations for $A_{85}B_{15}$ (up four figures) and $A_{15}B_{85}$ (bottom four figures). BF in the figures is just Γ_b

We can see that the "cherry-pit" structure can be observed on both sides of the phase diagram. However, for $A_{15}B_{85}$ alloy, when the "cherry-pit" are presenting, the values of Γ_b are smaller than the $A_{85}B_{15}$ case.

To quantify the difference, we calculated the structure factor, shown in Fig.6.

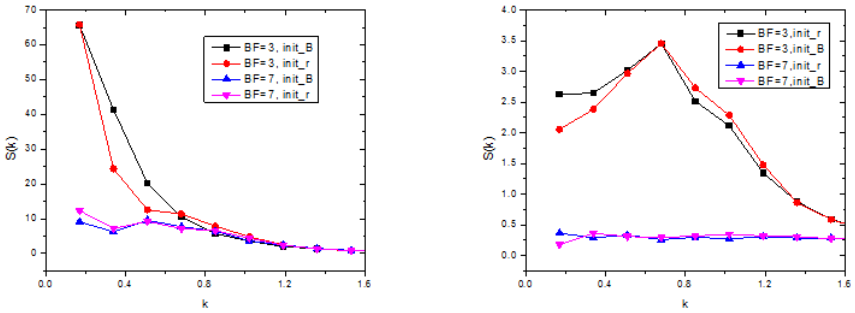

Figure 6: Structure factor for both $A_{85}B_{15}$ (left) and $A_{15}B_{85}$ (right) alloys. Simulation are run from different initial configurations(random solution and single B precipitate) to make sure steady state have been reached.

According to Enrique and Bellon's argument[8], alloy system under ion irradiation can be put into different regimes, by analyzing the structure factor. Enrique and Bellon have constructed a dynamical phase diagram, shown as Fig.7. Three regimes are defined: macroscopic phase separation, patterning, and solid solution.

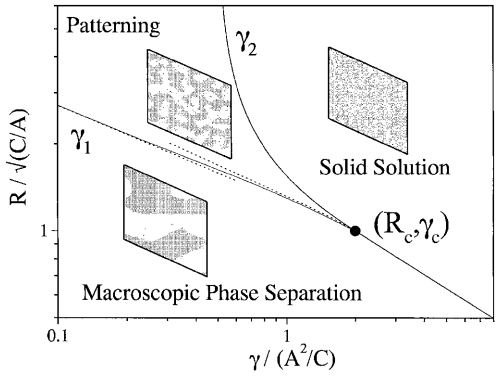

Figure 7: Steady-state regimes as a function of R and g. γ is the ration of Γ_b and the thermal atomic mobility. R is the relocation distance. Figure from [8].

From Fig.6, we know that for $\Gamma = 3s^{-1}$, $A_{85}B_{15}$ alloy lies in the macroscopic phase separation regime, while the $A_{15}B_{85}$ one lies in the patterning regime. Therefore obvious "cherry-pit" structure will only be found in the macroscopic phase separation regime. In addition, on different sides of the phase diagram, the alloy have different dynamical phase diagram, i.e., the boundary between macroscopic phase separation regime and the patterning regime is different. The solubility will change the dynamical phase diagram.

4.3 "pit" cluster size evolution

As we can see from Fig.5, the "pit" size varies from case to case. We would like to know how the "pit" evolute during the simulation. Do they keep almost the same size during the evolution or not? To answer this question, we keep track of the largest B precipitate in the simulation, and count the number of A atoms that are contained in the B precipitate during the simulation. We plot in Fig.8. the evolution of B precipitate size, A atom numbers, as well as the whole precipitate size(A+B cluster size), for $\Gamma_b = 0.7s^{-1}$.

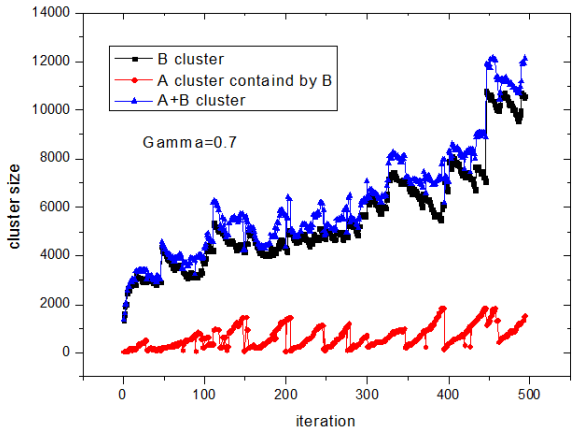

Figure 8: Largest B precipitate size evolution and the A atoms contained in the precipitate.

From Fig.8, we can see that the "pit" size is also evolution. By directly visualizing the evolution(video not shown here), there is a cycle of evolution of the "pit". At the beginning of the cycle, as A atoms being injected into the B precipitate (the cherry) by the ballistic jumps, the concentration of A atoms in the B precipitate increases. Then the "pit" nucleate at somewhere in the "cherry". Then the "pit" is stable and grows in size. At last, the cycle ends as the pit somehow touches the matrix and become a part of the matrix again. And the new cycle begins.

4.4 Cluster mobility

Formation of a cluster of certain component is always related to the mobility of that component. For example, in ion irradiated materials, gas bubble formation depends on the mobility of the gas (either in the form of individual atoms or complexes), the minimum number of gas atoms which are able to form a stable nucleus and the rate at which lattice vacancies can be supplied to enhance the stability of a nucleated core[9]. In this section we will try to find whether the mobility of clusters will affect the formation of such structures.

We will use KMC simulation to calculate mobility of clusters of different size. For single atom, we can also use the five-frequency model to calculate the mobility directly.

For KMC simulation, we use a $32\times32\times32$ simulation box in order to shorter the simulation time. Only pairwise interaction is used, in order to simplify the analysis. Two sets of cohesive

	ϵ^{order}	ϵ^{coh}_{AA}	ϵ^{coh}_{BB}	ϵ^{f}_{V}	ϵ^{saddle}
$A_{85}B_{15}$ set1	0.0553eV	-4.34eV	-4.34eV	1.28eV	-10.217eV
$A_{85}B_{15}$ set2	0.0553eV	-4.34eV	-4.174eV	1.28eV	-10.217eV

Table 2: All the energy parameters for cluster mobility simulation.

energy are chosen. One set of parameters (set1) will produce the "cherry-pit" structure, while the other set (set2) will not. The energies are tabulated as follows, in table.2.

To obtain similar average precipitate size, for parameter set 1, we use $\Gamma_b = 3s^{-1}$, and for parameter set 2, Γ_b is set to be $100s^{-1}$. Temperature is set to be T = 0.0408eV. The typical configuration for $A_{85}B_{15}$ alloy is shown in Fig.9.

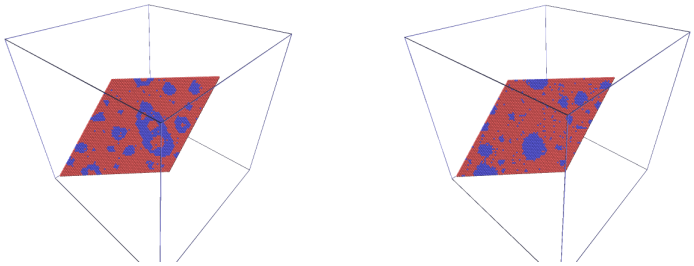

Figure 9: Steady-state configuration of KMC simulation using parameter set 1(left) and parameter set 2(right).

Cluster mobility (Diffusivity) is calculated using the formula

$$D =< r^2 > /6t$$

For clusters, $< r^2 >$ is the mean square displacement of the center of mass of the cluster. We follow Soisson *et al.*[10]. The simulation will start from a single A cluster inside the B matrix, in order to simulate the "pit" in "cherry" configuration and be performed with ballistic events absent to avoid rapidly emitting of atoms. However, for a single atom "cluster", we can turn on the ballistic exchange anyway. In the simulation, the ratio between local vacancy concentrations is controlled by the difference in vacancy formation energies, but the total concentration (1/N) is imposed. The physical time must be rescaled to take this into account[10]. The physical time is recaled according to

$$t = t_{MC} \frac{C_V^{MC}}{C_V^{eq}}$$

C_V^{MC} is the vacancy concentration in the matrix, calculated in the simulation. C_V^{eq} is the equilibrium vacancy concentration in pure B matrix, which can be calculated directly.

The cluster mobility will change as the cluster size changes. The simulation results are plotted in Fig.10 as mobility-cluster size relationship.

As we can see from Fig.10, for both case, compared with single atom behavior, the clusters are not mobile. More importantly, for the parameter set that will lead to "cherry-pit" structure, the mobility of clusters are significantly lower than the "no cherry-pit" case.

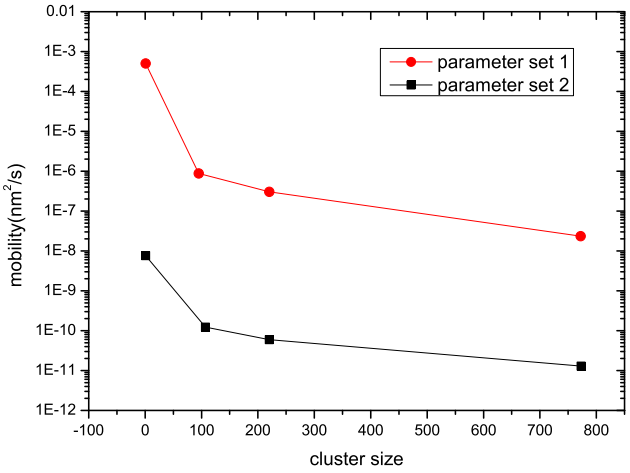

Figure 10: The mobility of cluster of a certain size drops significantly in the cherry-pit forming parameter(set 1). The four cluster size are 1, 110, 220, 770, approximately.

Simulations have shown that if we manually put a "pit" in a B precipitate and turn off the ballistic jumps, with both sets of parameters, the "pit" will finally disappear because of emitting of single atoms into the matrix. However, since the significant difference of single atom mobility (on the order of 10^5), the time needed for the process is different. With the ballistic jumps presenting, we have the source of A atoms, which can migrate in the B precipitate and join the "pit". However, for the no "cherry-pit" case, the injection rate is not high enough to reinforce A atoms. Therefore, for a given mobility, there should be a lowest value for Γ_b to provide enough injected A atoms to complement A atom in the "pit". However, too high Γ_b will lead to too small B precipitate, which will also prevent the "cherry-pit" structures to form.

4.5 Gibbs-Thomson effect and critical nucleation size

The GibbsCThomson effect relates surface curvature to vapor pressure and chemical potential and is a consequence of surface tension. A practical effect of Gibbs-Thomson effect is that the solubility of a phase depend on the particle size[11]:

$$\frac{X_r}{X_\infty} = \exp(\frac{2\gamma V_m}{RTr})$$

X_r and X_∞ are the solubility with a particle radius r and ∞ (flat interface, as considered in the semi grand canonical simulation). γ is the surface energy, and V_m is the molar volume of the phase.

For the particle itself, the Gibbs-Thomson effect will impose a critical size for the precipitate to be stable. That's why we select the second size of the cluster to be about 100 atoms to calculate the cluster mobility in previous section.

As for the "cherry-pit" structure formation, because of the Gibbs-Thomson effect, the concentration of the A atoms in B precipitate should be well beyond the solubility in order to nucleate a big enough "pit" that is not so mobile.

5 Conclusions

Kinetic Monte Carlo simulation has been shown to be a useful approach to study of binary alloy microstructure evolution under ion irradiation. Experimentally observed "cherry-pit" structures are reproduced in the model binary alloy system.

Two approached have been tried to rationalize the formation of such microstructure. We constructed asymmetry phase diagram by introducing triplet interactions, and ran simulations on both sides of the phase diagram. We draw the conclusion that if "cherry-pit" structure is presenting on one side of the phase diagram, it should also be observed on the other side, but with different Γ_b value. On different sides of the phase diagram, with the same simulation parameters, the system can be in different region of the dynamical phase diagram(see Fig.7).

Then we tried to see whether the mobility of clusters affect the formation of the "cherry-pit" structure. We found that the mobility of single atom is important. For a given mobility, there should be a lowest value for Γ_b to provide enough injected A atoms to complement A atom in the "pit". However, if the lowest limit of Γ_b is too high, B precipitate will be too small, and the "cherry-pit" structures will not form. Therefore, a low A atom mobility is crucial for "cherry-pit" structure to form.

References

[1] B. Stumphy. in preparation.

[2] Jia Ye. *Nanoscale patterning of chemical order introduced by displacement cascades in irradiated alloys*. PhD thesis, 2006.

[3] R. A. Enrique. *Phase and microstructural stability in immiscible binary alloys inder irradiation*. PhD thesis, 2001.

[4] R. S. Averback R. A. Enrique, K. Nordlund and P. Bellon. *J. Appl. Phys.*, 93:2917, 2002.

[5] P. Bellon M. Athenes and G. Martin. *Acta mater.*, 48:2675, 2000.

[6] J. G. Briano and E. D. Glandt. *J. Chem. Phys.*, 80:3336, 1984.

[7] F. E. Bernardi and G. C. Rutledg. *Macromolecules*, 40:4691, 2007.

[8] R. A. Enrique and P. Bellon. *Phys. Rev. Lett.*, 84:2885, 2000.

[9] P. R. Roy and D. N. Sah. *Solid state physics and materials science*, 24:397, 1985.

[10] F. Soisson and Chu-Chun Fu. *Phys. Rev. B*, 76:214102, 2007.

[11] K. E. Easterling D. A. Porter. *Phase Transformations in Metals and Alloys, Second Edition*. CRC Press, 1991.